J. Fluid Mech. (1990), *vol.* 215, *pp.* 585–599
Printed in Great Britain

Stability of a thin annular film in pressure-driven, low-Reynolds-number flow through a capillary

By R. W. AUL AND W. L. OLBRICHT†
School of Chemical Engineering, Cornell University, Ithaca, NY 14850, USA

(Received 17 March 1989 and in revised form 12 December 1989)

Experimental studies of low-Reynolds number, pressure-driven core–annular flow in a straight capillary tube are reported. The annular film is thin compared with the radius of the tube, and the viscosity of the film fluid is much larger than the viscosity of the core fluid. Photographs show that the film is unstable under all conditions investigated in the experiment. The film fluid collects in axisymmetric lobes that are spaced periodically along the capillary wall. The spacing of the lobes and their translational velocity correspond closely with the wavelength of the most unstable disturbance and phase velocity calculated from linear stability theory. Eventually, the continued growth of the lobes results in the formation of a fluid lens that breaks the inner core.

1. Introduction

One of the difficulties in analysing the flow of immiscible fluid mixtures in porous media is that the spatial distribution of the fluid phases in the porous matrix often is unknown. This distribution influences transport properties of the medium, including the relative mobilities of the fluids in response to an imposed pressure gradient. The spatial configuration of a given phase is strongly affected by its saturation in the medium. At sufficiently large saturations, a phase can be interconnected by fluid-conducting paths that extend over many pores. However, these paths are subject to flow-induced breakup and reformation, which can lead to changes in the relative mobility of the phase.

A prototype problem that has proven useful in understanding some of these phenomena is the motion of immiscible fluids through networks of pores where the dimensions of the pores and the topology of the network are known exactly. An experimental model can be made by etching a network of microscopic channels in a transparent substrate. The usual experiment is to fill all the channels with one fluid and then displace it by pumping an immiscible fluid through the network. The results show that residual thin films of the displaced liquid often are deposited along the walls of the channels, especially when a less viscous fluid displaces a more viscous one. However, the influence of these films on flow in a single channel is difficult to ascertain, because only the total flow rate through the network is known. Local flow rates are unsteady and vary among the channels in ways that depend on the network topology and the spatial distribution of the fluids.

The dynamics of a thin film deposited on a capillary wall by an advancing drop or bubble has been studied extensively, although mainly to predict the thickness of the deposited film as a function of flow rate and fluid properties. For the case of a long

† To whom correspondence should be addressed.

inviscid bubble displacing a viscous liquid in creeping flow, Bretherton (1961) and Park & Homsy (1984) found that the thickness of the deposited film, relative to the tube radius, varies with $Ca^{\frac{2}{3}}$ for small Ca, where the capillary number Ca gives the importance of viscous forces compared to forces due to interfacial tension. For the case of a long liquid drop that displaces an immiscible liquid, Schwartz, Princen & Kiss (1986) determined that the film thickness depends on $(3Ca)^{\frac{2}{3}}P$, where P is an $O(1)$ factor that depends on the viscosity ratio and on film thickness.

The present work is concerned with the stability of a thin film deposited by an advancing fluid when the viscosity of the advancing fluid is smaller than that of the fluid being displaced. It is well known that thin annular films are unstable under certain conditions. Goren (1962) showed that an initially stagnant film surrounding a wire or coating the inner wall of a tube is unstable to infinitesimal disturbances of wavelength greater than the circumference of the undisturbed film. The instability is driven by interfacial tension and the curvature of the interface caused by the disturbance.

For the case of an annular film surrounding an immiscible fluid core with an imposed pressure-driven flow, Hickox (1971) investigated the stability of the film to long-wavelength disturbances. Joseph, Renardy & Renardy (1984) and Hu & Joseph (1989) carried out comprehensive linear stability analyses of the core–annular flow, including effects of inertia in both phases. When the film viscosity is greater than the core viscosity, the wavelength of the most unstable disturbance is independent of Reynolds number Re for Re smaller than about 100. The wave speed is proportional to Re. Frenkel *et al.* (1987) showed that linearly unstable disturbances can be stabilized at sufficiently high flow rates, although the values of Ca and Re required for film stabilization are not likely to be achieved in the small pores under consideration in the present work.

Indeed, displacement velocities and pore sizes in oil recovery processes are sufficiently small that Ca and Re also are small. If a film forms on the capillary wall during displacement, the analyses mentioned above suggest that its thickness is small relative to the tube diameter, and this is confirmed by experiments. The film is unstable to small axisymmetric disturbances under these circumstances, and the wavelength and phase velocity of the disturbance can be calculated from a linear stability analysis. However, a linear analysis cannot determine the ultimate effect of the instability on the configuration of the fluids. The film may thin in certain locations along the capillary and eventually rupture, which leads to dewetting of the capillary wall. Alternatively, the film fluid may collect in lobes which form lenses bridging the capillary and breaking the core.

Hammond (1983) addressed exactly this issue for a thin viscous film without an imposed flow. The linear stability results in this case are unaffected by the presence of the core, but Hammond derived an evolution equation for the interface and integrated it numerically for film thickness variations outside the limits of validity of a linear analysis. This calculation shows that the film liquid collects in lobes spaced periodically along the tube wall. The film between these lobes continues to thin indefinitely, suggesting that it may eventually break, isolating the lobes from each other. Whether or not the film finally ruptures would depend on non-hydrodynamic forces not taken into account in the analysis but, in either event, the analysis shows that the core remains intact. Gauglitz & Radke (1988) used an approximation for the interface shape to extend the results of Hammond to thicker films. They found that if the film thickness is larger than some critical value, the capillary instability leads to pinch-off of the core rather than rupture of the film.

Previous experiments on the motion of long drops in straight circular capillaries have shown pinch-off of the core fluid, but not for the thin films under consideration here. Goldsmith & Mason (1963) studied the motion of large liquid drops suspended in creeping flow through capillaries with an interior diameter of 0.2 and 0.4 cm. The ratio of film thickness to tube radius varied between 0.19 and 0.36. The films surrounding the drops remained uniform in thickness provided the flow was maintained, but when the flow was stopped, a capillary instability developed in the film. In this case, the disturbances led to rupture of the liquid drop into a series of shorter drops.

The experiment described in §2 is designed to study the stability of a thin viscous annular film under an imposed flow. The film is produced by displacing a viscous liquid with an immiscible, less viscous liquid. To make sure the resulting film is thin, a capillary with a diameter of 54 μm is used. According to results from Schwartz, *et al.* (1986), the resulting film thickness should be about 1 μm. Although non-hydrodynamic forces such as van der Waals interactions should be insignificant for a film of this thickness, they may become important if the film thickness decreases during the flow. The influence of non-hydrodynamic forces on the linear stability of an annular film has been described by Aul (1989), and the results will be used to test whether such forces influence the dynamics of the film in the experiment.

2. Experimental

The core–annular flow, which is shown in figure 1, consists of an inner core of viscosity μ and undisturbed radius R_1 surrounded by an annular film of viscosity $\sigma\mu$ and undisturbed thickness h_0. The radius of the capillary is R_0. There are several ways to generate core–annular flow, but in view of the potential application to multiphase flow through porous media, a method was chosen that simulates the immiscible displacement of a viscous oil by a less viscous aqueous phase in a single pore.

2.1. *Experimental configuration and protocol*

The experimental set-up is shown in figure 2. The central part of the apparatus is a straight glass capillary tube of circular cross-section. The capillary is 2.5 cm in length and has an inner diameter of 54 ± 1 μm. The tube is cleaned with chromic acid and flushed with deionized water before starting the experiment.

The annular flow is generated by simultaneously pumping oil and water through the test section at precisely controlled flow rates. The flow is driven by a Sage Model 355 dual syringe pump equipped with a 10 μl syringe filled with oil and a 100 μl syringe filled with water. The fluids flow from the syringes through flexible Teflon tubes to a Plexiglass T-shaped manifold where they are combined. From the manifold, the immiscible mixture of oil and water flows through a Teflon tube to an entrance section, a glass capillary tube with an inner diameter of 190 μm. The entrance section is connected, in turn, to the test section. Thus, the oil–water mixture flows through a path that contains stagewise reductions in tube diameter from the large Teflon tube, to the 190 μm glass tube, and finally to the 54 μm test section. All connections between tubes in the system are permanently sealed to prevent leakage. The total flow rate of the two-phase mixture of oil and water is adjusted with the variable speed-pump, but the flow rate of water is ten times the flow rate of oil in every case, owing to the sizes of the two syringes. For these conditions, the flow between the manifold and the test section consists of alternating

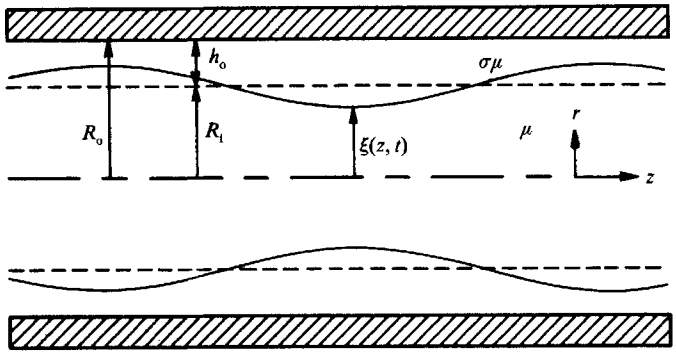

FIGURE 1. Schematic of the annular flow arrangement showing the perturbed interface.

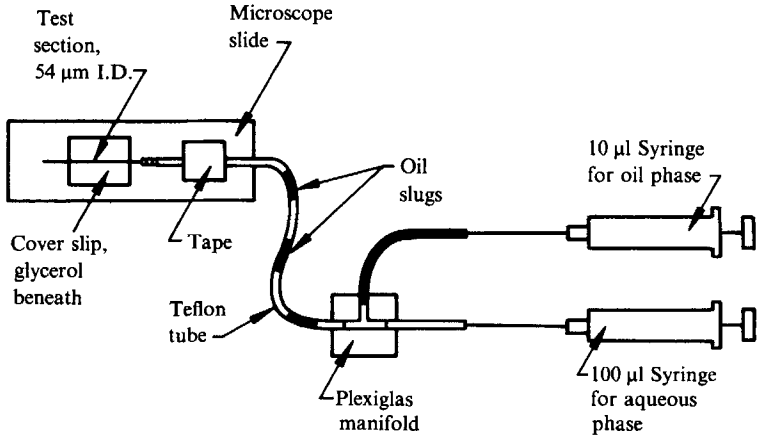

FIGURE 2. Schematic of the apparatus.

slugs of oil and water. The volume of each slug is much greater than the volume of the test section capillary.

Each experimental run begins with the test section filled with oil. A water slug enters the test section and displaces the oil, leaving a thin film of oil along the tube wall. Flow in the water slug and in the oil film closely approximates the annular flow shown in figure 1, except near the entrance to the capillary test section and near the leading edge of the water slug. The water slug eventually fills the entire length of the test section, and the dynamics of the thin oil film are observed. The run ends when the next oil slug enters the test section. In this experiment the viscous oil preferentially wets the capillary wall, and the oil slug displaces water in a piston-like motion until the tube is completely filled with oil. The experiment begins again when the next water slug enters the test section.

2.2. *Flow visualization*

The experimental arrangement permits repeated observations of the oil film as each successive pair of oil and water slugs flows through the test section. The oil film is viewed with a Zeiss microscope equipped with a motorized stage. The capillary test section is fixed to a microscope slide mounted on the stage, which is illuminated from

Film fluid	Core fluid	σ	V (μm/s)	Re	Ca	$Bo \times 10^5$
UCON LB-400X	Water	173	299	0.0080	0.015	1.6
UCON LB-400X	Water	173	448	0.012	0.022	1.6
UCON LB-400X	Water	173	697	0.019	0.034	1.6
UCON LB-170X	Water	80	448	0.012	0.010	2.3
UCON LB-70X	Water	19	448	0.012	0.0024	7.4

TABLE 1. Fluid systems and conditions of the experiment

below by a halogen lamp. To reduce optical distortion due to the glass wall, which has a refractive index of 1.474 at 25 °C, the test capillary is immersed in glycerol with a refractive index of 1.472, and held under a glass cover slip. The microscope image is displayed on a video-monitor, recorded on videotape, and photographed with a Nikon 35 mm camera attached to the microscope. Two objectives require effective magnifications of 160× and 100×. Details of the film shape can be resolved using the 160× magnification, but the length of the capillary in the viewing field is only about fifteen tube diameters. With the 100× magnification, the image contains a greater length of the film, but gives lower resolution of the interface shape. The entire length of the capillary can be scanned using the motorized stage at continuously adjustable speeds up to 1000 μm/s.

2.3. *Experimental materials and conditions*

The oils used in the experiment are Union Carbide polyalkylene glycols. The following grades are used to adjust the viscosity ratio: UCON LB-400X with a viscosity of 1.70 P and a density of 1.006 g/cm^3; UCON LB-170X with a viscosity of 0.79 P and a density of 0.988 g/cm^3; and UCON LB-70X with a viscosity of 0.19 P and a density of 0.962 g/cm^3. The refractive indices of the UCON oils are between 1.45 and 1.46. The core fluid in all cases is deionized water. The ratios of film fluid viscosity to core fluid viscosity are 173, 80, and 19 for the three UCON oil films. The interfacial tension γ measured with a DuNuoy tensiometer is 3.5 dyne/cm for the UCON/water systems.

Experimental conditions are summarized in table 1. Most of the experiments were conducted for a total flow rate that gives an average velocity of 448 μm/s in the test section. Owing to the small test section diameter, the Reynolds number based on the core fluid and the imposed velocity is always smaller than 0.019. The capillary number Ca, defined here as $\sigma\mu V/\gamma$, varies over the range $0.0024 \leqslant Ca \leqslant 0.034$. The Bond number Bo, defined as $\Delta\rho g R_0^2/\gamma$ where $\Delta\rho$ is the difference in density between the fluids, is at most 7.4×10^{-5}, which suggests that effects of non-neutral buoyancy are negligible.

3. Experimental results and discussion

The results of the experiment are displayed in a series of photographs that show the time evolution of the thin viscous film. Quantitative measurements of the film thickness as a function of time and the phase velocity of disturbances also are presented. Although oil and water slugs pass repeatedly through the channel during the experiment, there is no discernible change in the film dynamics with time.

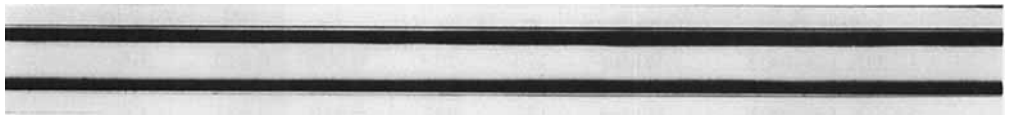

FIGURE 3. An unperturbed thin film of oil on the capillary inner wall ($R_0 = 27$ μm) for $\sigma = 173$, $Ca = 0.022$, $V = 448$ μm/s. The core fluid is water.

3.1. *Film shape*

Figure 3 is a photograph of the annular flow in the test section during the displacement of oil by water. The flow is from left to right in the photograph, which was taken at an arbitrary point along the test section about one second after the leading edge of the water slug passed the microscope objective. For this case, the capillary number is 0.022 and the viscosity ratio σ is 173.

Because the illumination source is on the opposite side of the capillary from the microscope objective, a shadowgraph of the core, i.e. the water slug, is obtained. Light passes through the central portion of the water core to the microscope objective, but light that passes through the edge of the water core does not reach the objective, owing to a difference in the refractive indices of water and glass. Thus, the image of the water core contains a dark shadow band that extends to the water–oil interface. A thin film of oil between the water core and the inner tube wall is discernible in the photograph. As far as can be determined from the photograph, the film thickness is independent of axial position, and its thickness, measured through the microscope, is 1.8 ± 0.5 μm. The uncertainty in the measurement is a consequence of the resolution of the microscope; errors due to slight difference in the refractive indices of the fluids are small, by comparison. The analysis of Schwartz *et al.* (1986) predicts a value of 2.8 μm for the conditions of the experiment.

Within several seconds a variation in film thickness can be discerned. The film becomes distributed into axisymmetric lobes or collars spaced periodically along the tube, as shown in figure 4. Although they cannot be seen in the photograph, lobes form along the entire length of the water slug, except in the vicinity of the leading edge of the slug. The wavelengths of the lobes shown in figure 4 are 248, 223, 223, and 223 μm. By using the motorized stage to translate the capillary, the wavelengths of many lobes can be measured rapidly. The wavelength of most of the lobes varies between 200 and 280 μm, although a few lobes have wavelengths as small as 130 μm. The average wavelength for the conditions shown in figure 4 is 225 μm. The axial velocity of the lobes measured from video recordings is smaller than 0.1 μm/s.

Similar experiments were carried out with the same fluid system for two other flow rates, 299 and 697 μm/s. These cases also show an evolution of lobes in the annular film similar to those shown in figure 4. The wavelength of the lobes for $\sigma = 173$ is not affected by the flow rate.

The experiment was also run with two less viscous oils that gave viscosity ratios σ of 80 and 19. For an average velocity of 448 μm/s, the measured undisturbed film thicknesses in these cases are 1.6 and 1.0 ± 0.5 μm, respectively. The time evolution of the film shape is qualitatively similar to that described above for the more viscous film. The measured average wavelength for $\sigma = 80$ is 225 μm, the same value as measured for the more viscous film. The average wavelength for $\sigma = 19$ is 250 μm. For a fixed flow rate the measured wave speeds of the lobes vary between 0.2 and 0.7 μm/s for $\sigma = 80$ and between 1 and 2.5 μm/s for $\sigma = 19$. The wave speed is

FIGURE 4. A view of the interface at 100× magnification showing the formation of periodically spaced lobes or collars for $\sigma = 173$ and $Ca = 0.022$. The flow is from left to right in the photograph.

proportional to the overall flow rate, but the average wavelength is independent of flow rate.

3.2. *Comparison with linear stability*

A linear stability analysis, e.g. Hu & Joseph (1989) and Aul (1989), of the core–annular flow shown in figure 1 shows that the film is unstable to axisymmetric disturbances with dimensionless wavenumber kR_i for $kR_i < 1$. The imposed flow does not affect the growth rate of small disturbances, regardless of the film thickness, but it does impart a phase velocity to the disturbance.

Aul (1989) included effects of van der Waals forces, which may modify the shape of the core–film interface for sufficiently thin films. The van der Waals forces produce a disjoining pressure in the film, which is given by Chen (1984) to within an additive constant as $-B/h^4$ for films thicker than about 400 Å. For thinner films, the disjoining pressure scales with h^{-3}. If B is positive, the disjoining pressure is negative, corresponding to an attractive force between the film–wall and film–core interfaces.

An explicit expression for the growth rate can be obtained in certain limits. The case of a very thin, viscous film, defined by

$$R_o = R_i(1+\epsilon) \quad \text{and} \quad \epsilon \ll \sigma, \tag{1}$$

is relevant to the experiments. The dimensionless growth rate is given by

$$\mathrm{Re}\,(s)\frac{R_i\sigma u}{\gamma} = \tfrac{1}{3}\epsilon^3(kR_i)^2[1-(kR_i)^2+C_v], \tag{2}$$

where $\mathrm{Re}\,(s)$ is the real part of the exponential growth coefficient s, and

$$C_v = \frac{4B}{\gamma R_o^3}\frac{(1+\epsilon)^3}{\epsilon^5} \tag{3}$$

is the ratio of van der Waals forces to interfacial tension forces that drive the instability. The wavelength of the fastest growing disturbance λ_d is

$$\lambda_d = 2^{\frac{3}{2}}\pi R_o(1+\epsilon)^{-1}(1+C_v)^{-\frac{1}{2}}. \tag{4}$$

The phase velocity of this disturbance turns out to be the same as the velocity at the undisturbed interface to within an error of ϵ^2/σ.

With little information available to estimate the value of the constant B, we take the same value used by Chen, 10^{-19} erg cm, and use the experimental values $R_o = 27$ μm and $\gamma = 3.5$ dyne/cm to illustrate the effects of non-hydrodynamic forces on the disturbance growth rate. Figure 5 shows the dimensionless growth rate of a small disturbance with wavenumber kR_i for two very small values of the initial film thickness. The dimensionless parameter C_v for $h_o = 0.1$ μm and $h_o = 0.2$ μm is 8.24 and 0.257, respectively. The force between the film interface and the tube wall is attractive, which promotes the growth of small disturbances. For these values of the parameters, the growth rate increases as the initial film thickness is made smaller,

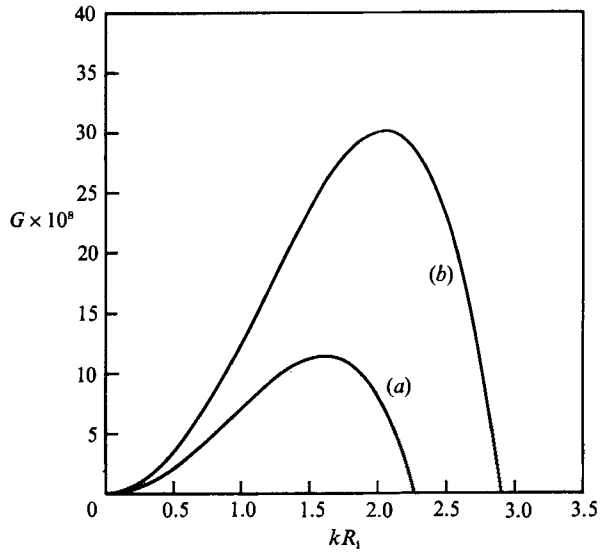

FIGURE 5. Dimensionless growth rate G as a function of dimensionless wavenumber kR_1: (a) $h_0 = 0.1$ μm, $\epsilon = 0.00372$, $C_v = 8.24$; (b) $h_0 = 0.2$ μm, $\epsilon = 0.00746$, $C_v = 0.257$.

because the increase in the attractive force between the core–film interface and the capillary wall is more than sufficient to make up for the increased viscous resistance to flow within the film. Figure 6 shows the wavelength of the fastest growing disturbance as a function of the undisturbed film thickness h_0.

The thickness at which van der Waals forces are significant may be overestimated, probably because of the uncertainty in the value of B. If the actual value of B is smaller than 10^{-19} erg cm, then the onset of the qualitative effects shown in figures 5 and 6 is shifted to thinner films. However, it is unlikely that nonhydrodynamic effects will be observed in the present experiment. Even with B set to 10^{-19} erg cm, the film must be very thin for van der Waals forces to be significant, and the growth rates in figure 5 for such thin films are very small.

In the experiment, the dimensionless thickness h_0/R_0 of the film is determined by parameters of the flow, namely the viscosity ratio σ and capillary number Ca. For the measured initial film thickness h_0, the predicted wavelength and wave speed of the most unstable disturbance for $C_v = 0$ are compared with experimental measurements in table 2 for an average velocity of 448 μm/s. The value of h_0 is known only to within 0.5 μm. Therefore, ranges of predicted values for the wavelength and wave speed are shown, which span the uncertainty in the film thickness measurement.

Although the measured values of the wavelength are close to the values predicted by linear stability theory, the measured wave speed is smaller than the predicted value in every case, even taking into account the uncertainty in the film thickness. In fact, for $\sigma = 173$ the lobes are practically stationary along the capillary wall, despite a predicted velocity of about 1 μm/s, which is sufficiently large to be measured in the experiment. On the other hand, the measured lobe velocity decreases as the viscosity ratio σ is made larger, which is in qualitative agreement with the linear analysis.

A discrepancy between the measured wave speeds and the calculated values is not surprising, since the linear analysis applies to perturbations in film shape that are

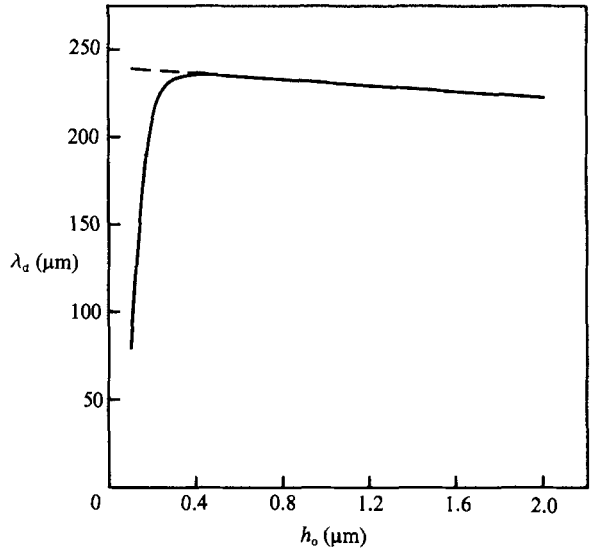

FIGURE 6. Dominant wavelength λ_d as a function of the undisturbed film thickness h_0: ----, $C_v = 0$; ——, $C_v = C_v(h_0)$.

			Predicted values		Measured values	
Ca	σ	h_0 (μm)	Wavelength (μm)	Wave speed (μm/s)	Wavelength (μm)	Wave speed (μm/s)
0.022	173	1.8	221–228	0.64–1.37	225	< 0.1
0.010	80	1.6	221–230	1.12–2.60	225	0.2–0.7
0.0024	19	1.0	227–235	1.91–6.88	250	1.0–2.5

TABLE 2. Comparison of the measured wavelength and wave speed with predictions of linear stability

much smaller than the undisturbed film thickness. Although the wave-speed measurements are made as soon as perturbations in the film can be discerned, the amplitude of the perturbations already exceeds the limits of the linear analysis. Furthermore, a detailed analysis of the videorecordings for very long times shows that the wave speed of an individual lobe decreases as the amplitude of the lobe increases. It is thus likely that at least part of the variation in the wave speed data in table 2 reflects the decreasing phase velocity over the course of the measurements.

3.3. *Breakup of the film and aqueous core*

Hammond (1983) calculated numerically the time-dependent shape of a thin viscous annular film subject to periodic axisymmetric disturbances of finite amplitude without an imposed flow. The calculation shows that the film drains into periodically spaced lobes while the interior core remains intact. Changes in the film shape take place over the time $(R_0\sigma\mu/\gamma)\,(h_0/R_0)^{-3}$, but the time required for the film to break between lobes is infinite in the absence of non-hydrodynamic forces. Aul (1989) carried out analogous calculations for an annular film with an imposed flow. For

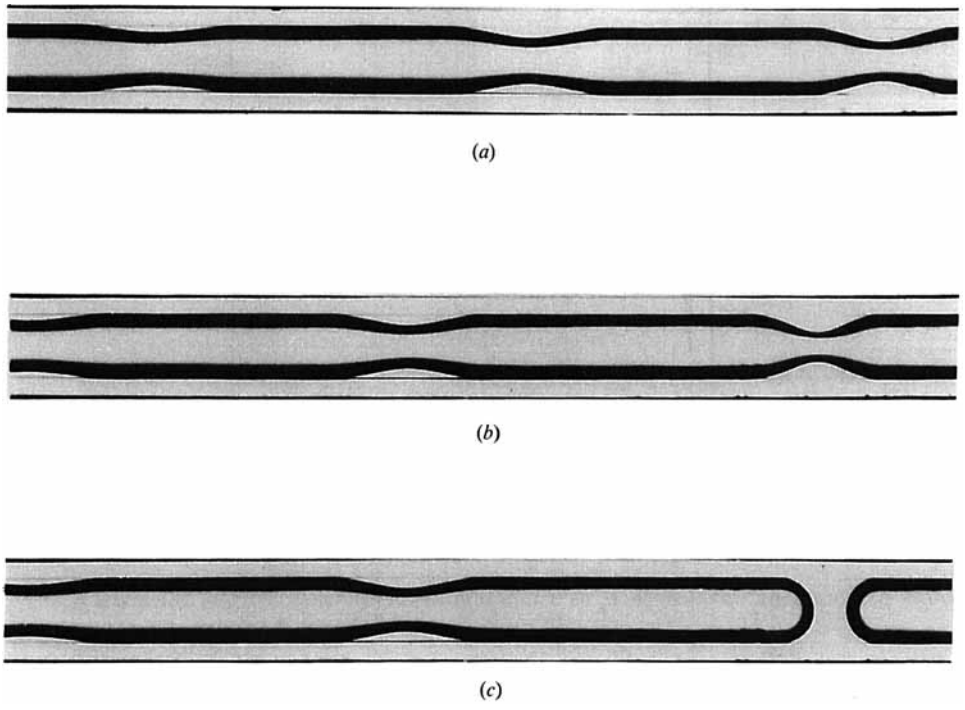

FIGURE 7. Pinch-off of the water core by lens formation for $\sigma = 173$, $V = 448$ μm/s and $Ca = 0.022$. The time between photographs (*a*) and (*b*) was 50 s, and the time between photographs (*b*) and (*c*) was 20 s.

conditions relevant to the experiments, the imposed flow affects the shape of the draining film, but it does not significantly affect the time for drainage.

Breakup of the film is not observed in the present experiment. Instead, the lobes grow until pinch-off of the water core occurs at one of the lobes. Figure 7 contains a sequence of photographs showing the formation and growth of lobes, and pinch-off of the water core for a case with $\sigma = 173$. The amplitudes of the lobes increase monotonically over a time of 50 s in the photographs in figure 7 (*a*, *b*). During this time, the capillary translates on the motorized stage to keep the same lobes in view. At a critical value of the lobe amplitude, one of the lobes suddenly forms an oil lens that occupies the entire cross-section of the capillary and causes a separation of the water core. The photograph in figure 7 (*c*) shows the oil lens immediately after its formation, which occurred 20 s after the photograph in figure 7 (*b*) was taken. The newly formed oil lens translates downstream with the average velocity of the two-phase flow, 448 μm/s.

Hammond (1983) and Gauglitz & Radke (1988) considered the possibility of pinch-off of the core fluid without an imposed flow. Hammond calculated the long-time drainage of fluid into the lobes from the flattened regions between the lobes. The velocity in the regions between lobes is small, because resistance to flow scales with h^{-3}, where h is the local film thickness. The details aside, the important points for present purpose are that transport of film fluid can occur only over an axial distance of $2\pi R_0$, and there is not enough fluid volume in the film over this distance for the lobes to form a lens. However, the volume of oil contained in the lobe that forms the

lens shown in figure 7 exceeds the volume of oil contained in a length $2\pi R_0$ of the unperturbed film, even considering the uncertainty in the film thickness measurement. Gauglitz & Radke (1988) extended Hammond's results, at least in an approximate manner, to thicker films. They found that when the film thickness exceeds $0.12R_0$, there is sufficient volume in the film for lens formation and pinch-off of the interior core. Their experiments with a gaseous interior core show that lens formation and pinch-off occurs without an imposed flow for films that are thicker than $0.09R_0$.

The important feature in the present experiment is that lens formation and breakup of the core are enhanced by transport of oil within the film due to the imposed flow. Since the total volumetric flow rate is constant and the form of the velocity profile in the film is known, the volumetric flux in the film can be calculated for a specified film thickness. For example, with a viscosity ratio of 19, the film thickness is about 1 μm for an average velocity of 448 μm/s. The volumetric flow rate of oil, estimated by integrating the undisturbed velocity profile across a film of constant thickness h_0, is 340 $\mu m^3/s$. This can be compared to the rate at which the volume of the lobe that ultimately forms a lens increases prior to pinch-off. The videorecordings show that the longitudinal cross-section of the lobe resembles a triangle with a height equal to the lobe amplitude and a base about $3.2R_0$ in length. Figure 10 below (for the first water slug) shows the lobe height as a function of time up to pinch-off. The corresponding rate of change in lobe volume just before pinch-off is 190 $\mu m^3/s$. This estimate suggests that transport in the film due to the imposed flow can supply the extra fluid required for the growth of a single lobe to pinch off, while surrounding lobes grow at a lesser rate. This is consistent with the shape of the film shown in figure 7. Although the lobes have similar amplitudes in the early stages of growth in figure 7 (*a*), eventually a single lobe grows faster than the others in figure 7 (*b*) and forms a lens that ruptures the water core. The rate of lens formation is sensitive to the imposed flow rate, but in any event pinch-off of the interior core with an imposed flow occurs for the thinner films than in the absence of flow. For example, for $\sigma = 19$ and $V = 448$ μm/s the measured film thickness at pinch-off of the core with an imposed flow is $0.04R_0$.

Although the entire capillary cannot be viewed at once, there is no evidence that the oil film ruptures anywhere in the test section. Instead, for the lobes to grow and form an oil lens, the film must remain intact. Therefore, the film at the entrance to the test section must be continuously supplied with oil that is transported to the sites of lobe formation. This supply of oil comes from an oil film that is clearly visible in the 190 μm entrance capillary upstream of the test section. The film in the larger tube supplies oil to the film in the test section.

3.4. *Formation of secondary lobes*

Occasionally, a secondary lobe forms between two lobes, as shown in figure 8. Although secondary lobes are smaller in amplitude than the primary lobes, they form at the same time as the primary lobes form. This eliminates the possibility that the secondary lobes reflect an instability at a reduced wavelength owing to a negative van der Waals disjoining pressure. For this to occur the film thickness in the vicinity of the secondary lobe must be less than about 0.1 μm, as demonstrated in figure 6. However, the lobe formation time for a film thickness of 0.1 μm is several orders of magnitude larger than the observed time in the experiment. A more likely possibility is that the secondary lobe corresponds to a satellite lobe predicted in the nonlinear analysis by Hammond (1983) and in analogous computations by Aul (1989) with an

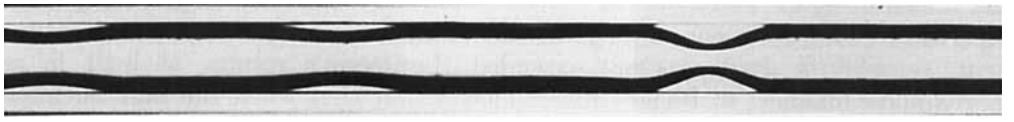

FIGURE 8. The formation of a small-amplitude secondary lobe, barely visible in the photograph, between two primary lobes for $\sigma = 173$, $V = 448$ μm/s and $Ca = 0.022$.

imposed flow. These results show that the timescale for secondary lobe formation coincides with the linear instability timescale for this flow, which is consistent with the experimental observation. In previous experimental studies, Goren (1962) reported observations of satellite lobes for the flow of an annular film surrounding a thin wire.

3.5. *Effects of lens formation on drop motion in the capillary*

Figure 9*b* shows the flow of two water slugs separated by an oil lens that formed from pinch-off of the water core shown in figure 9(*a*). The film surrounding the downstream slug has lobes extending upstream to the lens. The axial velocity of these lobes is smaller than 0.1 μm/s, compared to the lens axial velocity of 448 μm/s. On a few occasions when the end of the water slug reaches an especially large lobe, the slug sheds a water drop of diameter $2R_0$. As the lens separating the two water slugs moves downstream, it collects oil from each nearly stationary lobe, and the volume of the oil lens increases. Because the photograph shows only the leading edge of the second slug, there are no lobes in the film surrounding it. Nevertheless, this film is unstable, too, and lobes are visible farther upstream out of the field of the photograph.

To determine whether the presence of the lens influences the film surrounding the upstream slug, the growth rates of lobes in the films surrounding *both* slugs were measured. Figure 10 shows the amplitudes of the lobes in the two films as a function of time for a viscosity ratio of 19 and a capillary number of 0.0024. The zero of time corresponds to the instant when the amplitude was sufficiently large to be measured on the video monitor. The lobe amplitudes in both films increase linearly with time, which suggests that the initial exponential growth due to a linear instability cannot be resolved in the experiment. Numerical calculations of the film shape for the experimental conditions given in figure 10 predict linear growth in time (Aul 1989).

A striking and unexpected result in figure 10 is the large difference in growth rates for the two films. Lobes in the downstream film grow faster than lobes in the upstream film by about a factor of three. Although it is difficult to measure the absolute thickness of the films, it is clear under the microscope that the *undisturbed* film surrounding the upstream slug is thinner than the *undisturbed* film surrounding the downstream slug. This difference in film thickness may account for the measured difference in growth rates, because changes in the film thickness scale with h_0^4. In any event, it is clear that the presence of the oil lens affects the thickness of the film surrounding the upstream slug.

The difference between the values of h_0 for the two films may be a consequence of the flow fields near the leading edges of the two slugs. Bretherton (1961) and Park & Homsy (1984) calculated the thickness of the thin film deposited by the motion of a single inviscid bubble through a capillary. Their results show that the film thickness depends on the local velocity and pressure fields near the leading edge of the bubble. In the experiment, the flow around the leading edge of the downstream

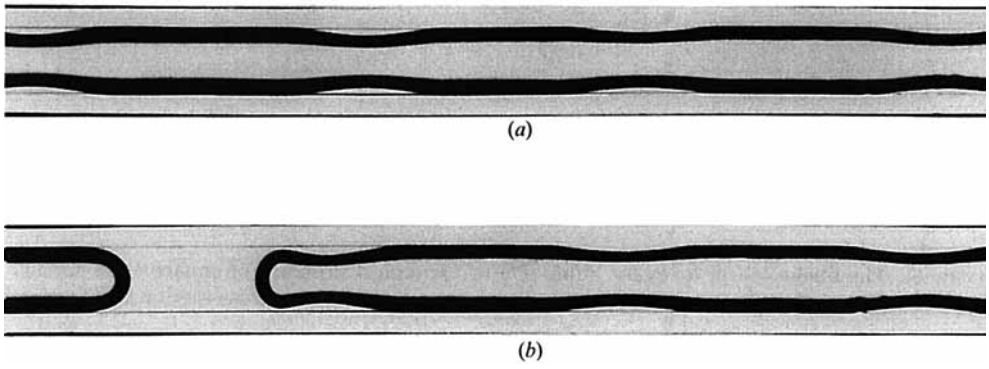

FIGURE 9. The rear end of a water slug and the leading edge of another water slug flowing from left to right for $\sigma = 173$ and $Ca = 0.022$. The axial velocity of the lobes is much smaller than the average fluid velocity.

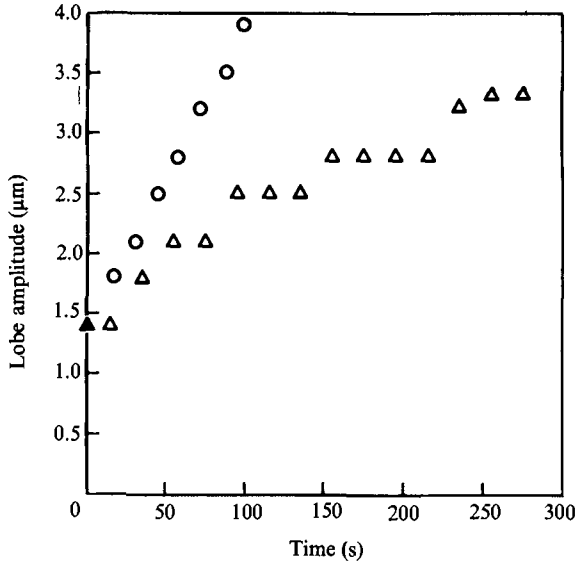

FIGURE 10. Growth rates of lobe amplitudes in the film surrounding two water slugs for $\sigma = 19$ and $Ca = 0.0024$: ○, first water slug in series; △, second water slug in series.

slug resembles the situation described by Bretherton and Park & Homsy, except, of course, that the bubble is a liquid drop with finite viscosity. Poiseuille flow is recovered sufficiently far downstream in the oil phase. However, when the lens separating two slugs is only one or two tube diameters in length, the velocity field within the lens resembles a bolus flow. It is likely that the bolus motion in the lens affect conditions near the leading edge of the upstream slug, and this may account for the smaller film thickness surrounding the upstream slug.

3.6. *Effect of capillary shape*

A typical flow channel in a real porous matrix has a complicated cross-sectional shape that varies in the direction of flow. Therefore, the shape of the capillary is often

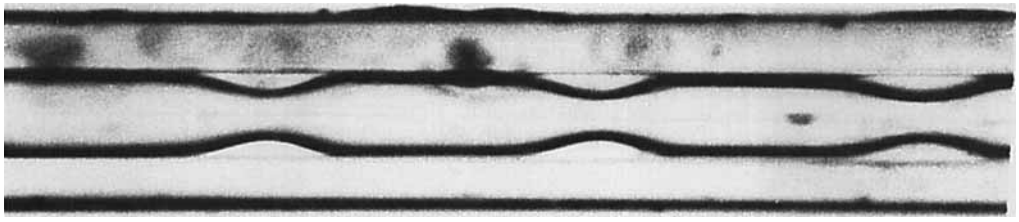

FIGURE 11. The formation of lobes for annular flow through a capillary of square cross-section for $\sigma = 173$ and $Ca = 0.0022$. The length of each side of the square cross-section is 50 μm.

treated as a parameter of multiphase flow experiments. For example, Arriola, Willhite & Green (1983) and Ransohoff, Gauglitz & Radke (1987) studied the flow of drops or bubbles in capillaries with a square cross-section. The local cross-section for channels in etched capillary networks (e.g. Lenormand, Zarcone & Sarr 1983, Li & Wardlaw 1985*a*, *b*, Chen 1986, Chen & Koplik 1985), is generally non-circular and often resembles a square.

To study the effects of cross-sectional shape on the stability of the film, a series of experiments were carried out in a capillary with square cross-section 50 μm in width. The annular film exhibits the same qualitative behaviour described above for circular capillaries, including formation of lobes, translation of the lobes in the direction of the average velocity, and pinch-off of the water core. Figure 11 shows lobe formation in a square capillary for a viscosity ratio of 173 and an average velocity of 450 μm/s. The measured average wavelength in this case is 190 μm.

Axial variations in the capillary shape were not considered explicitly in the present experiment, but experiments in etched capillary networks show that abrupt changes in the cross-sectional geometry can strongly affect pinch-off of a non-wetting phase. Li & Wardlaw (1985*b*) and Chen & Koplik (1985) used networks consisting of nearly spherical cavities called pores connected together by long narrow channels of uniform diameter called throats. As the non-wetting phase advances through the network, snap-off occurs in the throats, but it takes place most often within one or two diameters of the throat entrance. Although most measurements of snap-off at sudden constrictions are mainly qualitative, Wardlaw (1982) and Lenormand *et al.* (1983) used single pore–throat pairs to show that snap-off can occur at a pore–throat junction, even without any visible evidence of lobe formation in the rest of the film. It is likely that the irregular shape of the boundary introduces finite-amplitude disturbances in the film shape when the non-wetting phase advances through the constriction, and these may expedite the growth of capillary instabilities.

4. Conclusions

An instability in core–annular flow at low Reynolds number has been demonstrated experimentally for thin films when the film fluid is more viscous than the core fluid. The film fluid gathers into lobes or collars that are spaced periodically along the length of the capillary. The observed wavelength of lobe formation and the translational velocity of the lobes agree reasonably well with linear stability results, even though the disturbance cannot be observed until its amplitude is comparable with the undisturbed film thickness.

In this experiment, the instability always results in the formation of a lens and

pinch-off of the water core. The imposed flow apparently enhances transport of the film fluid to a lobe which grows faster than its neighbours and eventually forms a lens. This result is in contrast to previous theoretical studies in the absence of an imposed flow, which show that a viscous film thins indefinitely, inhibiting transport of fluid in the film. However, breakup of the film is never observed in the present experiment.

The present experiments were conducted for a fixed flow rate. In a real porous medium, such as a model composed of etched networks of channels, the pressure drop across any channel is fixed. During an immiscible displacement, local velocities and flow rates throughout the porous network fluctuate in time in response to changes in the fluid composition of the matrix. If annular films are present and the network geometry permits long-wavelength disturbances, the final outcome of the annular film instability still depends on the local flow rate. In channels where the flow in the film due to the pressure difference across the channel is comparable in magnitude with the flow induced by the capillary instability, the film may form a lens that results in snap-off of the core. In channels where the pressure-driven film flow is much smaller in magnitude than the capillary-induced flow, the theoretical results of Hammond should apply, and the film will thin indefinitely, until non-hydrodynamic forces become important.

REFERENCES

ARRIOLA, A., WILLHITE, G. P. GREEN, D. W. 1983 *Soc. Petrol. Engrs J.* Feb. 1983, 99.

AUL, R. W. 1989 The motion of drops and long bubbles through small capillaries: coalescence of drops and annular film stability. Ph.D. thesis, Cornell University, Ithaca, NY.

BRETHERTON, F. P. 1961 *J. Fluid Mech.* **10**, 166

CHEN, J.-D. 1984 *J. Colloid Interface Sci.* **98**, 329.

CHEN, J.-D. 1986 *J. Colloid Interface Sci.* **110**, 448.

CHEN, J.-D. & KOPLIK, J. 1985 *J. Colloid Interface Sci.* **108**, 304.

FRENKEL, A. L., BABCHIN, A. J., LEVICH, B. G., SHLANG, T. & SIVASHINSKY, G. I. 1987 *J. Colloid Interface Sci.* **115**, 225.

GAUGLITZ, P. A. & RADKE, C. J. 1988 *Chem. Engng Sci.* **43**, 1457.

GOLDSMITH, H. L. & MASON, S. G. 1963 *J. Colloid Interface Sci.* **18**, 237.

GOREN, S. L. 1962 *J. Fluid Mech.* **12**, 309.

HAMMOND, P. S. 1983 *J. Fluid Mech.* **137**, 363.

HICKOX, C. E. 1971 *Phys. Fluids* **14**, 251.

HU, H. & JOSEPH, D. D. 1989 *J. Fluid Mech.* **205**, 359.

JOSEPH, D. D., RENARDY, M. RENARDY, Y. 1984 *J. Fluid Mech.* **141**, 369.

LENORMAND, R., ZARCONE, C. & SARR, A. 1983 *J. Fluid Mech.* **135**, 337.

LI, Y. & WARDLAW, N. C. 1985*a* *J. Colloid Interface Sci.* **109**, 461.

LI, Y. & WARDLAW, N. C. 1985*b* *J. Colloid Interface Sci.* **109**, 473.

PARK, C.-W. & HOMSY, G. M. 1984 *J. Fluid Mech.* **139**, 291.

RANSOHOFF, T. C., GAUGLITZ, P. A. & RADKE, C. J. 1987 *AIChE J* **33**, 753.

SCHWARTZ, L. W., PRINCEN, H. M. & KISS, A. D. 1986 *J. Fluid Mech.* **172**, 259.

WARDLAW, N. C. 1982 *J. Can. Petrol. Tech.* May–June, 21.